



Hypsometric control on surface and subsurface runoff

Enrique R. Vivoni,¹ Francesco Di Benedetto,¹ Salvatore Grimaldi,²
and Elfatih A. B. Eltahir³

Received 18 February 2008; revised 5 August 2008; accepted 30 October 2008; published 31 December 2008.

[1] A fundamental problem in hydrology is relating the basin hydrological response to the geomorphologic properties of a catchment. In this technical note, we show that the hypsometric distribution exerts control on surface and subsurface runoff partitioning by isolating its effect with respect to other basin characteristics. We conduct simulations using a distributed watershed model for hypsometric realizations developed by modifying the contour line values of a real basin. Results indicate that the runoff components are a function of the basin hypsometric form. In general, a relatively less eroded (convex) basin exhibits higher total runoff that is more dominated by subsurface processes, while a relatively more eroded (concave) basin shows less total runoff with a higher fraction of surface response. Hypsometric differences are also observed in the relations between base flow discharge and the mean groundwater depth and the variable source area. Furthermore, the hypsometric form reveals clear signatures on the spatial distribution of soil moisture and runoff response mechanisms.

Citation: Vivoni, E. R., F. Di Benedetto, S. Grimaldi, and E. A. B. Eltahir (2008), Hypsometric control on surface and subsurface runoff, *Water Resour. Res.*, 44, W12502, doi:10.1029/2008WR006931.

1. Introduction

[2] Quantitative analysis of the physical connections between geomorphologic structure and hydrologic response has been pioneered by *Rodriguez-Iturbe and Valdes* [1979]. The hydrological response of watersheds to precipitation events depends on the mechanisms of runoff generation, in particular on the partitioning between surface and subsurface discharge to the channel network. Previous studies have suggested that topography plays a significant role in determining the basin response [e.g., *Howard*, 1990; *Marani et al.*, 2001; *Bertoldi et al.*, 2006]. Furthermore, the dominant runoff mechanisms can also impact the outcome of erosional processes on landscape form [e.g., *Ijjász-Vásquez et al.*, 1992; *Tucker and Bras*, 1998]. As a result, a strong interplay exists between basin geomorphic shape and its hydrological response.

[3] While hydrological processes depend on many basin properties, the relief ratio and catchment volume play important roles in determining runoff [e.g., *Zecharias and Brutsaert*, 1988; *Luo and Harlin*, 2003]. The relief ratio (R_r , defined as the maximum elevation difference divided by the longest flow path) indicates the overall steepness of a basin and controls lateral water redistribution, while the catchment volume (V_c , defined as the amount of mass above a datum) provides a measure of storage capacity and determines locations of groundwater seepage. Variations in R_r

and V_c are anticipated to impact both surface and subsurface runoff components.

[4] The relief ratio and catchment volume can be concisely captured through the hypsometric (area-altitude) curve, the cumulative (or exceedence) distribution of basin area with elevation. Introduced by *Langbein et al.* [1947] and *Strahler* [1952], the hypsometric curve is typically represented as the distribution of the relative height (h/H) with relative area (a/A). Despite that the hypsometric curve aggregates the three-dimensional basin structure, its shape has been related to the hydrograph peak and travel time [*Harlin*, 1984; *Luo and Harlin*, 2003], the regional groundwater base flow [*Marani et al.*, 2001], and the dominant erosion process [*Moglen and Bras*, 1995; *Willgoose and Hancock*, 1998; *Luo*, 2000]. Further, the hypsometric curve has been widely used to interpret stages of landscape evolution due to uplift and denudation [e.g., *Strahler*, 1952; *Ohmori*, 1993; *Willgoose and Hancock*, 1998].

[5] Field studies of the effect of basin hypsometry on runoff partitioning have not been conducted owing to the difficulty in isolating terrain controls from other important factors (e.g., climate, soils, vegetation). *Luo* [2000] found through a topographic analysis of 45 basins that the hypsometric curve could distinguish landscapes dominated by surface or subsurface runoff. This study suggests that the hypsometric distribution contains information on the dominant runoff mechanism. Numerical simulations that capture topographic variations, while isolating other factors, can be invaluable for exploring this aspect of the basin response. For example, model simulations of the impact of runoff mechanisms on landscape evolution and basin hypsometry have yielded considerable insight [e.g., *Ijjász-Vásquez et al.*, 1992; *Tucker and Bras*, 1998].

[6] In this technical note, we study the variation in runoff partitioning for realizations of the same basin with forms representing varying development stages. The hypsometric

¹Department of Earth and Environmental Science, New Mexico Institute of Mining and Technology, Socorro, New Mexico, USA.

²Dipartimento di Geologia e Ingegneria Meccanica, Naturalistica e Idraulica per il Territorio, Università degli Studi della Tuscia, Viterbo, Italy.

³Department of Civil and Environmental Engineering, Massachusetts Institute of Technology, Cambridge, Massachusetts, USA.

realizations are synthetically generated to mimic long-term evolution without accounting for changes in soil, channel or vegetation distributions. A distributed watershed model [Ivanov *et al.*, 2004a] is used to discriminate between surface and subsurface runoff over a sequence of storm and interstorm periods (see Vivoni *et al.* [2007] for an analysis of the simulated runoff partitioning). Antecedent wetness conditions imposed through a distributed water table are also varied to explore its effect on runoff response for the various hypsometric surfaces. We identify how the hypsometric curve influences prestorm surface saturation and the water table position, the basin water balance, runoff partitioning, and the spatial distribution of soil moisture and runoff generation.

2. Methods

2.1. Basin Hypsometric Distributions

[7] The hypsometric curve can be readily obtained from a grid or contour representation of surface topography. In this study, we use the U.S. Geological Survey digital elevation model (DEM) at 30 m resolution of the Peacheater Creek at Christie, OK (64 km²) (Figure 1a). Given its location in the Ozark Plateau, the southern part is fluviably dissected, while the northern portion is a gently sloping upland characterized by a plateau and a remnant high peak. Elevations vary from 248 m near the outlet to 432 m at the high ridge in the northeast. The configuration of the upland plateau and the dissected lowlands lends itself to imposing hypsometric changes to the basin that mimic the effects of long-term landscape evolution, as performed in numerical experiments [e.g., Willgoose, 1994; Moglen and Bras, 1995].

[8] The Peacheater Creek is a humid, perennial basin with mean annual rainfall of ~1200 mm, distributed in two wet periods (March to June, and September to November) [Vivoni *et al.*, 2007]. Major floods in the basin are due to frontal storms with high rainfall intensities occurring in the spring and fall seasons. The basin response is composed of a mixture of surface and subsurface discharge due to frequent storm-induced flood events and the base flow generated from the shallow underlying aquifer [Imes and Emmett, 1994]. Reed *et al.* [2004] and Ivanov *et al.* [2004b] attribute the characteristics and seasonality of the observed and simulated streamflow response to the multiple runoff mechanisms in the Peacheater Creek. As a result, the terrain setting and runoff mechanisms in the basin are appropriate for quantifying hypsometric controls.

[9] Figure 1b compares the hypsometric curve of Peacheater Creek (labeled Original) with two alternative representations. A simple procedure was used to alter the elevation values of the contour lines, while preserving their two-dimensional (plan view) horizontal structure. The original 30 m DEM was first converted to a contour line representation with 10 m vertical intervals. The contour intervals (e.g., the actual elevation labels associated with a contour line) were then varied to produce a Convex and a Concave surface. This was achieved by varying the contour line elevation labels in a geographical information system. To preserve the relief ratio, R_r , we imposed a 5 m contour interval at low elevations (i.e., 248 to 340 m of the Original surface) and a 15 m spacing at high elevations (i.e., 340 to 432 m) to generate the Convex surface. This leads to an

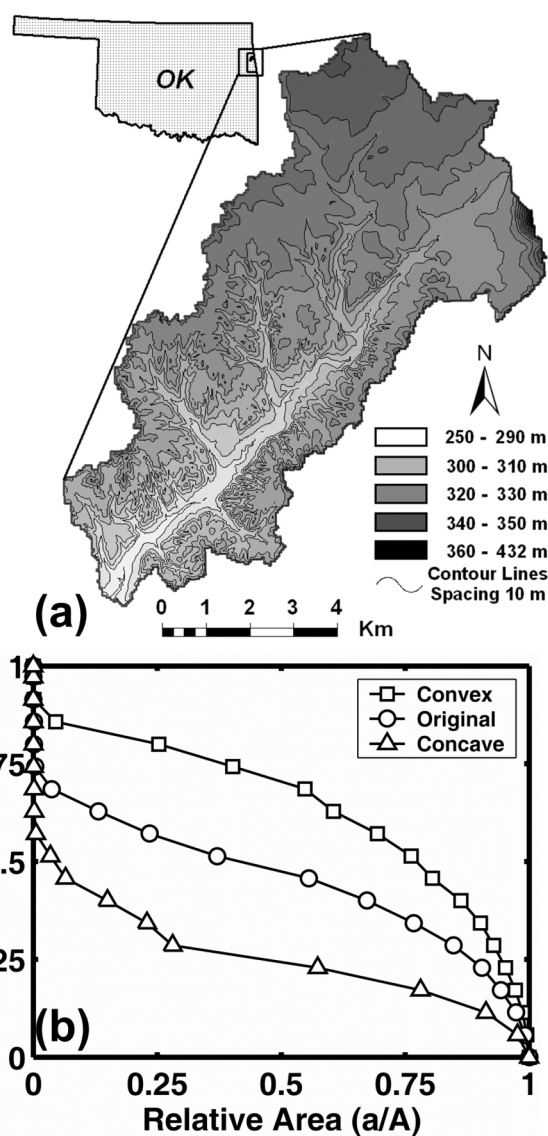


Figure 1. Surface topography and hypsometric form for the Peacheater Creek basin in Oklahoma. (a) Terrain representation using 50-m DEM and contour lines at 10-m spacing (mean elevation of 325 m, standard deviation of elevation of 26.6 m, and elevation range of 184 m). (b) Hypsometric curves for the three realizations of the Peacheater Creek basin: Convex, Original, and Concave surfaces. The hypsometric distribution is depicted as the relative height (h/H) versus the relative area (a/A), where a is the area of basin above height h , A is the total basin area, h is the height above the basin outlet, and H is the total relief of the basin.

increase in the total basin area found at high altitudes. Conversely, contour intervals of 15 m at low elevations and 5 m at high elevations were used for the Concave surface. While other variations to the contour intervals are possible, this simple procedure changes the hypsometric curve and matches the relief ratio of the Original surface.

[10] Subsequently, contour line maps were interpolated to a 10 m raster grid to preserve the major features and then resampled using a cubic convolution algorithm to a 50 m

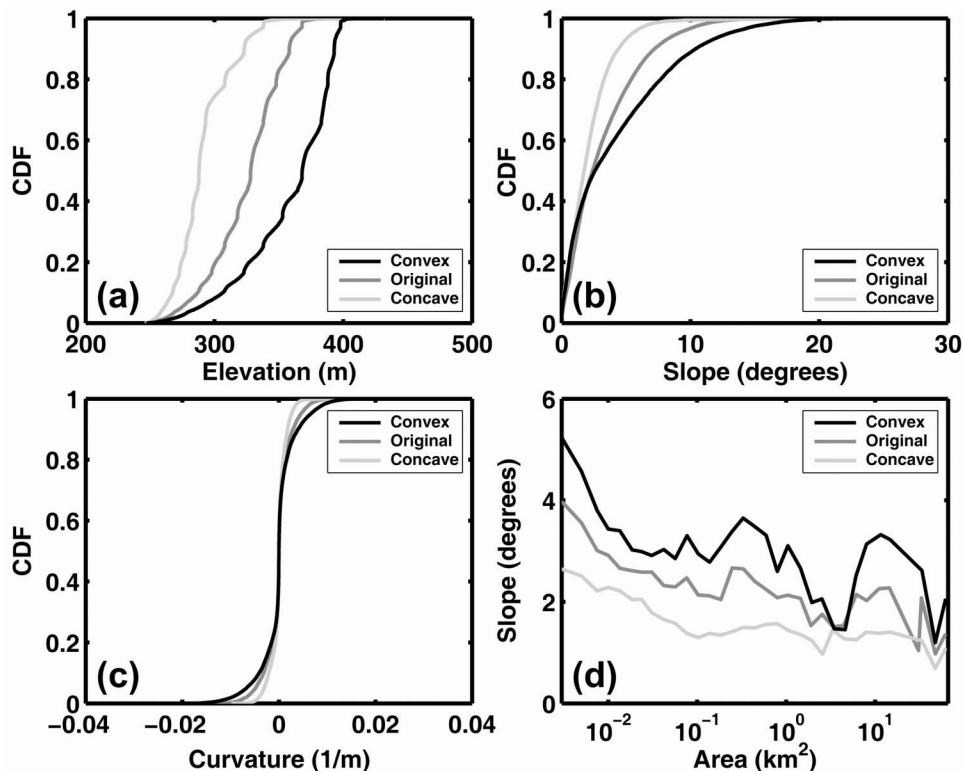


Figure 2. Terrain attributes for the three hypsometric realizations of the Peacheater Creek basin at 50-m resolution. (a) Cumulative distribution function (CDF) of the basin elevation (m). (b) CDF of the basin slope (degrees). (c) CDF of the basin curvature ($1/m$). (d) Slope-area relation calculated using the bin-averaged slope (degrees) and contributing (upslope) area (km^2). The bin width varied along the logarithmic scale used for the area (ranging from 2.5×10^{-3} to $66 km^2$). Note that the channel network is defined for areas greater than $0.51 km^2$ in each surface.

DEM for the purposes of computational efficiency. Given the elevation modifications performed, the three 50 m DEMs were corrected hydrologically to remove sinks [Hutchinson, 1989]. We verified the three surfaces retained similar relief ratio (R_r) and the distribution of upslope contributing area in the basin (not shown). Distributions of elevation, slope, curvature and the slope-area relation for each realization were inspected (Figure 2). Clearly, hypsometric modifications led to expected changes in the elevation distribution, while minor variations were imposed on the curvature. Slope distributions varied considerably among the surfaces owing to changes in the contour intervals, resulting in clear differences in the slope-area relation, but reasonably similar scaling exponents [Tarboton *et al.*, 1992] for upslope areas from 0.5 to $64 km^2$. Relative to the Original, the Convex basin has a larger fraction of area at high elevations and higher slopes at lower elevations, while the Concave surface has greater basin area and lower slopes at lower altitudes.

[11] The hypsometric curves capture the Young (Convex), Mature (Original) and Monadnock (Concave) stages described by Strahler [1952]. As a result, the hypsometric distributions are considered to represent a range of observed conditions within a wider natural variability [e.g., Strahler, 1952; Schumm, 1956]. Differences of the hypsometric surfaces can be also quantified using the statistical metrics introduced by Harlin [1978]: hypsometric integral (I), skewness (SK) and kurtosis (K); and density skewness

(DSK) and kurtosis (DK), as shown in Table 1. These parameters provide quantitative insight into the geomorphic differences among the realizations and allow comparison to other studies. For example, the progressive decrease in I for the Convex, Original and Concave basins, reflects the removal of catchment volume, V_c . Further, an important difference is captured by DSK with positive (negative) density skewness for the Concave (Convex) surface, pointing to high erosion amounts in the upper (lower) basin regions.

2.2. Watershed Modeling for Runoff Partitioning

[12] The hypsometric realizations are used as a terrain condition for simulations using the triangulated irregular network (TIN)-based Real-time Integrated Basin Simulator (tRIBS) [Ivanov *et al.*, 2004a]. tRIBS is a fully distributed hydrological model that uses a TIN to represent topography and its hydrographic features, including the stream network and basin boundary [Vivoni *et al.*, 2004]. The distributed model captures variations in topography, soils, vegetation, and atmospheric forcing at fine spatial and temporal resolutions. Hydrological states and fluxes are computed using the Voronoi cells surrounding each TIN node which form a finite-volume domain. For consistency, we created fine-resolution TINs for each hypsometric surface preserving 90% of the cells in the 50-m DEMs. This ensured that spatial sensitivity due to topographic resolution was avoided among the simulations, as discussed by Vivoni *et al.* [2005].

Table 1. Statistical Parameters for the Three Hypsometric Surfaces Computed Using *Luo* [1998]^a

Hypsometric Surface	<i>I</i>	<i>SK</i>	<i>K</i>	<i>DSK</i>	<i>DK</i>
Convex	0.640	0.236	1.964	-0.784	2.119
Original	0.457	0.296	1.927	-0.032	1.269
Concave	0.262	0.420	1.829	0.904	1.982

^a*I* is the hypsometric integral, *SK* is the hypsometric skewness, *K* is the hypsometric kurtosis, *DSK* is the density skewness, and *DK* is the density kurtosis. Each parameter (dimensionless) is based on the hypsometric curve and its density function, defined as the rate of change of the hypsometric curve (see *Harlin* [1978], *Luo* [1998], and *Luo and Harlin* [2003] for details). *I* quantifies the catchment volume and is computed as the area underneath the hypsometric curve. *SK* and *K* capture the spatial distribution of erosion development and are obtained as the normalized third and fourth moments of the hypsometric distribution. Similarly, *DSK* and *DK* are computed as the normalized third and fourth moment of the hypsometric density function and describe the spatial distribution of basin relief.

[13] A key model characteristic is its simulation of surface-subsurface dynamics in the interconnected hillslope and channel system [*Ivanov et al.*, 2004a]. Basin hydrologic response is modeled by tracking infiltration fronts, water table fluctuations and lateral soil moisture fluxes impacted by surface topography and soil characteristics. Runoff can be generated via infiltration-excess (R_I), saturation-excess (R_S), perched return flow (R_P) and groundwater exfiltration (R_G) mechanisms depending on the precipitation characteristics, landscape attributes and prior wetness conditions in the basin (see *Vivoni et al.* [2007] for a detailed discussion). Runoff produced by surface and subsurface mechanisms is transported overland by hydrologic hillslope routing and kinematic wave channel routing. Evaporation from bare soil and intercepted rainfall, and plant transpiration are computed from radiation and energy balance calculations performed using meteorological data. Owing to the coupled surface-subsurface processes, the distributed model has been successfully applied for continuous simulations in large river basins [*Ivanov et al.*, 2004a, 2004b; *Vivoni et al.*, 2005, 2007]. Further, *Ivanov et al.* [2004a] discussed the reliability of the surface and subsurface runoff partitioning produced by the distributed model.

[14] Hydrological simulations ensured that basin characteristics, other than topography, were consistent for the three hypsometric surfaces. Soil, vegetation and channel network parameters were determined through calibration exercises described by *Vivoni et al.* [2005] for the Original surface using several years of Next Generation Weather Radar (NEXRAD) rainfall and U.S. Geological Survey streamflow data [see *Vivoni et al.*, 2005, Table 3]. A similar channel network with identical drainage density was enforced to reduce potential effects on the runoff travel times introduced by having differences in the network geometry. Specifically, a constant area threshold of 0.51 km² was used to define the stream channels to match the observed hydrography in the Original surface [*Vivoni et al.*, 2005]. A plane bedrock surface, placed 10 m below the lowest elevation in the basin, was used as a consistent lower, impermeable boundary. We carried out a drainage experiment (~4 years) for each hypsometric realization to obtain initial water table conditions corresponding to high, intermediate and low base flow, as determined from streamflow data (see *Vivoni et al.* [2007] for details on the model initialization). A spin-up period was not conducted (as done by *Vivoni et al.* [2005])

as our interest here is on how the interaction of the initial water table position and hypsometric form influence the partitioning of surface and subsurface runoff. One-year simulations were then carried out using hourly rainfall data from NEXRAD (~4 km by 4 km) and surface meteorological forcing from a nearby weather station. While the simulation is relatively short (November 1997 to 1998), the period samples a series of major storms [*Vivoni et al.*, 2005] and is sufficient to discern the hypsometric controls on the runoff response. In the following, we first inspect the hypsometric control on the groundwater and surface saturation conditions obtained during the drainage experiment.

3. Results and Discussion

3.1. Hypsometric Control on Groundwater and Variable Source Area Rating Curves

[15] Groundwater rating curves capture the physical link between base flow (Q_b) and the mean depth to the water table (N_{wt}). Several studies have identified nonlinearities in the $Q_b - N_{wt}$ relation [e.g., *Duffy*, 1996; *Eltahir and Yeh*, 1999]. *Marani et al.* [2001] suggested that basin hypsometry plays a role in the observed nonlinearity via interactions with the water table position. Figure 3a compares the groundwater rating curves obtained by draining each surface from a saturated condition ($N_{wt} = 0$ at $t = 0$). Subject to no atmospheric forcing, subsurface gravity drainage leads to increasing N_{wt} , resulting in decreasing Q_b through the outlet. A stronger base flow decrease is observed when the water table depth is close to the ground surface. As the water table interaction with topography weakens, Q_b decreases at a slower rate. This behavior indicates that the model reproduces the significant degree of nonlinearity in the groundwater rating curve, as observed by, for example, *Duffy* [1996] and *Eltahir and Yeh* [1999]. While a strong nonlinearity is apparent in each surface, hypsometric differences impact the groundwater rating curve, with a shallower (deeper) N_{wt} sustaining an equivalent Q_b for the Concave (Convex) basins, suggesting a stronger (weaker) connection between topography and the water table.

[16] Figure 3b shows the relation between base flow discharge and the saturated area (A_s) for each surface. This “variable source area rating curve” depicts seepage sites where the water table intersects the land surface. As the water table deepens and Q_b decreases, seepage faces become smaller in area. Note, however, that the form of the variable source area rating curve is distinct from the $Q_b - N_{wt}$ relation, having a more gradual decrease in Q_b for large A_s . Nonlinearity is still observed in the $Q_b - A_s$ relation, with a change occurring for small base flow. Hypsometric differences are more pronounced for high base flow, with a progressively larger A_s for the Convex, Original and Concave surfaces. This is consistent with the topographic control on the $Q_b - A_s$ relation identified through several field studies (see *Latron and Gallart* [2007], in particular their Figure 8). As observed in comparing Figures 3a and 3b, it is clear that the Concave (Convex) surface with a shallower (deeper) N_{wt} is associated with a higher (lower) A_s at an equivalent Q_b . This implies that a particular base flow can be achieved via gravity drainage by different combinations of N_{wt} and A_s for varying hypsometric surfaces. As a result, the hypsometric form determines the mean depth to

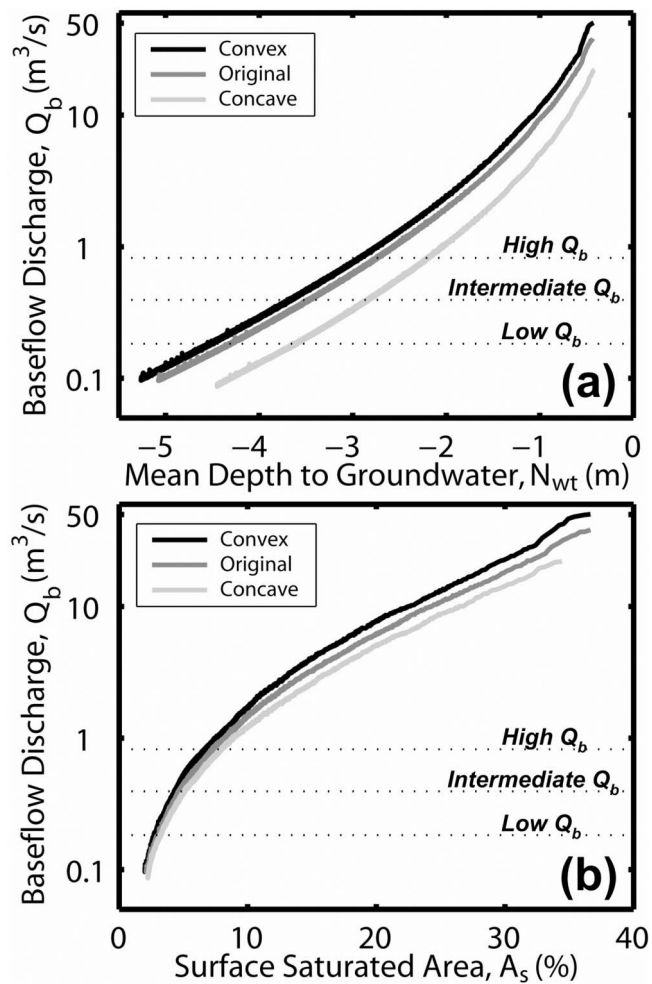


Figure 3. Variation of surface and subsurface conditions with base flow discharge (Q_b in m^3/s) during drainage experiments for the three hypsometric realizations. (a) Spatially averaged depth to the water table position (N_{wt} in m). N_{wt} is measured from the land surface ($z = 0$) and is more negative for deeper water table positions. (b) Percentage of surface saturated area in the basin (A_s in %). The three horizontal lines represent high ($0.82 m^3/s$, 75th percentile), intermediate ($0.39 m^3/s$, 50th percentile), and low ($0.18 m^3/s$, 25th percentile) base flow conditions prior to storm events derived from observed USGS discharge at Peacheater Creek (1993–2003).

groundwater and the surface saturated area in the basin. Changes in the initial wetness can influence the storm runoff response, as described in the following.

3.2. Hypsometric Control on Basin Water Balance and Runoff Partitioning

[17] The annual water balance, $\Delta S = P - ET - R$, and the runoff partitioning into surface and subsurface flow, $R = R_I + R_S + R_P + R_G$, can quantify the impact of hypsometry on the basin response. To isolate the hypsometric effect, initial water table positions were selected at three constant base flow levels (high, intermediate and low) from the drainage experiment (Figure 3). Table 2 presents the basin water balance for the three initial conditions (or antecedent wetness based on the water table position in the model [see

Ivanov *et al.*, 2004a]). Large differences are observed in runoff (R), evapotranspiration (ET) and change in storage (ΔS) for the hypsometric surfaces given the same precipitation (P). The Concave (Convex) basin has a higher (lower) ET , but lower (higher) R as compared to the Original surface. This suggests that hypsometry affects the basin water balance and supports conclusions on topographic effects presented by Bertoldi *et al.* [2006] for another region. We note that R is more sensitive to changes in hypsometry and antecedent wetness as compared to ET . Further, changes in total runoff (R) exhibit a larger (smaller) sensitivity to the initial wetness for the Convex (Concave) surface as compared to the Original basin. Specifically, the change in R from high to the low initial conditions ($\Delta R = R_{high} - R_{low}$) is greater for the Convex basin ($\Delta R = 159 mm$) than the Concave basin ($\Delta R = 142 mm$).

[18] The runoff sensitivity to basin hypsometry is accompanied by changes in the distribution of surface ($R_I + R_S$) and subsurface ($R_P + R_G$) components at the annual scale. Figure 4a shows the runoff fractions for the intermediate base flow ($Q_b = 0.39 m^3/s$). Note the increase in surface runoff and decrease in subsurface runoff from the Convex to the Concave basins. Similar behavior is observed for the low and high initial base flow conditions, as quantified in Table 3. Differences in the runoff partitioning can be related to the statistical properties of the hypsometric distribution. The less eroded Convex basin exhibits higher I , lower SK and a negative DSK , which favor the production of subsurface seepage (R_P) as noted by Luo [2000]. The more eroded Concave surface has a lower I , higher SK and positive DSK , indicating that low slope areas exist toward the basin outlet [Harlin, 1984]. Low slope, near channel regions in the Concave basin are observed to generate higher R_S and R_I in equal proportions, suggesting that saturated surface areas lead to frequent R_S and that low surface gradients enhance R_I . The impact on infiltration excess runoff is due to the reduced lateral moisture transport in the Concave basin, which prevents rapid dissipation of shallow saturation that leads to R_I [see Vivoni *et al.*, 2007]. Note that the groundwater exfiltration (R_G) does not appear to be sensitive to the

Table 2. Water Balance Components for the Three Initial Conditions (or Antecedent Wetness Related to the Groundwater Distribution) in Each Hypsometric Surface Computed Over the 1-Year Simulations, 1 November 1997 to 31 October 1998^a

Hypsometric Surface	Initial Condition	P (mm)	ET (mm)	R (mm)	ΔS (mm)
Convex	low	1181	985	281	-85
	intermediate	-	1005	362	-186
	high	-	1015	440	-274
Original	low	1181	994	262	-75
	intermediate	-	1014	339	-172
	high	-	1025	413	-257
Concave	low	1181	1026	246	-91
	intermediate	-	1043	310	-172
	high	-	1055	388	-262

^a P , ET , R , and ΔS are the basin-averaged precipitation, evapotranspiration, outlet runoff, and change in storage, expressed as depths (mm). The change in storage is calculated from the other components and is negative since the water table positions facilitate high losses ($ET + R$) as compared to precipitation input. The low ($Q_b = 0.18 m^3/s$), intermediate ($Q_b = 0.39 m^3/s$), and high ($Q_b = 0.82 m^3/s$) initial conditions are compared.

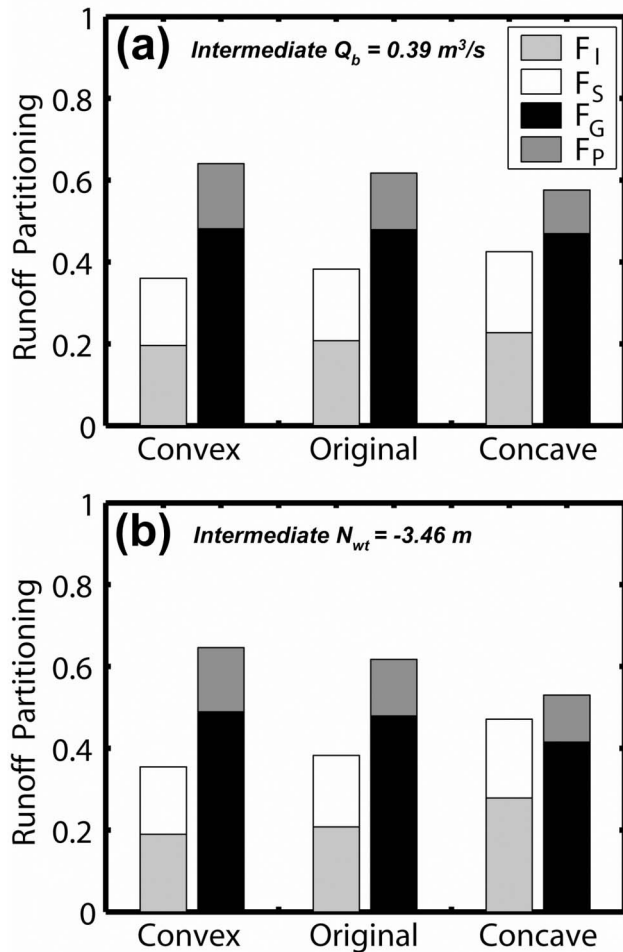


Figure 4. Runoff partitioning for the three hypsometric realizations for two different initial conditions. Initialization at a constant Q_b isolates the sensitivity to hypsometric form, while the constant N_{wt} initial condition captures the combined effect of hypsometry and antecedent wetness. The total runoff volume (R) is partitioned into the fraction of infiltration-excess runoff ($F_I = R_I/R$), saturation-excess runoff ($F_S = R_S/R$), perched return flow ($F_P = R_P/R$), and groundwater exfiltration ($F_G = R_G/R$). (a) Initial water table position at the intermediate base flow level ($Q_b = 0.39 \text{ m}^3/\text{s}$) for the Convex ($N_{wt} = -3.65 \text{ m}$), Original ($N_{wt} = -3.46 \text{ m}$), and Concave ($N_{wt} = -2.83 \text{ m}$) surfaces. The total runoff varies for each case: Convex ($R^* = 1.07$) and Concave ($R^* = 0.92$), where R^* is the total runoff for the particular case normalized by the total runoff from the Original surface. (b) Initial water table position set at $N_{wt} = -3.46 \text{ m}$ for the Convex ($Q_b = 0.49 \text{ m}^3/\text{s}$), Original ($Q_b = 0.39 \text{ m}^3/\text{s}$), and Concave ($Q_b = 0.21 \text{ m}^3/\text{s}$) basins. The total runoff varies for each case: Convex ($R^* = 1.10$) and Concave ($R^* = 0.75$). This initialization corresponds to the value of N_{wt} for the intermediate base flow in the Original surface.

hypsometric form for the constant initializations at the low, intermediate or high base flows (Table 3).

[19] To test the trends in the hypsometric differences, we inspected the runoff partitioning at the event scale by selecting four floods for the intermediate base flow (not

shown). Events were chosen to vary in terms of the season of occurrence, to completely contain the rising and recession limbs, and to differ in peak discharge (Q_p ranging from 6 to 28 m^3/s). Results indicated that (1) event scale trends in runoff partitioning across the hypsometric surfaces matched the annual trends (see Figure 4a) and (2) variations existed in the relative amounts of each runoff mechanism for individual events (e.g., winter events were more subsurface dominated than fall floods). The analysis did not demonstrate a reversal of the runoff partitioning sensitivity to topographic form as shown by Bertoldi *et al.* [2006] from the annual to the event scales.

[20] Figure 4b compares runoff partitioning for the three surfaces initialized with a similar mean groundwater depth ($N_{wt} = -3.46 \text{ m}$). This initial water table leads to different Q_b in each surface, thus allowing for varying levels of antecedent wetness. As a result, we observe larger differences in runoff partitioning between the Convex and Concave surfaces. In particular, the Concave basin exhibits a large decrease ($\sim 25\%$) in total R , while the Convex basin has a modest increase ($\sim 10\%$) in R relative to the Original. The differences are primarily attributed to subsurface mechanisms ($R_P + R_G$) as the water table position changes with respect to the land surface. Clearly, the water table plays a critical role in determining subsurface contributions, which can amplify the runoff partitioning sensitivity to hypsometric form. To confirm this trend, simulations at high (low) Q_b exhibited higher (lower) subsurface runoff due to increased (decreased) $R_G + R_P$ contributions (Table 3). Similar trends in the hypsometric control on the runoff partitioning for the constant initial water table were obtained for the selected flood events (not shown). As a result, the interaction of the hypsometric form and the water table position should influence the spatial distribution of runoff generation.

3.3. Hypsometric Control on Spatial Soil Moisture and Runoff Generation

[21] The spatial distribution of basin response can reveal the hypsometric control on hydrological states and fluxes. To illustrate the hypsometric signature, we determine the spatial differences between the Convex and Concave surfaces. For reference, Figure 5a presents the elevation difference ($\Delta z = z_{\text{Convex}} - z_{\text{Concave}}$) between the two hypsometric realizations. Note the areas of high elevation change along midbasin positions, while the headwaters and outlet exhibit small variations in altitude. Changes in the elevation distribution propagate to the basin response. Figure 5b shows the difference in time-averaged surface soil moisture (Δs), an integrated measure of the hydrologic state in each basin location. The spatial pattern of Δs reveals that the less eroded Convex basin has higher wetness in the incised channel network (see b1), while the more eroded Concave surface exhibits higher soil moisture in the broad and relatively flat valley regions (b2). This suggests that the Convex (Concave) surface has more concentrated (dispersed) soil moisture at shallow depths along the channel network as compared to the Original surface. The frequency distribution of Δs indicates that 65% of the basin displays negative values, implying the Concave surface has a higher surface wetness extended over a larger region.

[22] A similar approach is used to quantify the hypsometric control on spatial runoff generation using the time-averaged surface and subsurface runoff rates (r in mm/hr).

Table 3. Runoff Partitioning for the Three Initial Conditions in Each Hypsometric Surface^a

Hypsometric Surface	F_I			F_S			F_P			F_G			R^*		
	Q_{bL}	Q_{bI}	Q_{bH}												
Convex	0.25	0.20	0.16	0.16	0.16	0.16	0.18	0.16	0.15	0.41	0.48	0.53	1.07	1.07	1.06
Original	0.27	0.21	0.17	0.17	0.17	0.17	0.15	0.14	0.13	0.41	0.48	0.53	1	1	1
Concave	0.29	0.23	0.18	0.19	0.20	0.20	0.11	0.10	0.09	0.41	0.47	0.53	0.94	0.92	0.94

^aThe three initial conditions are $Q_{bL} = 0.18 \text{ m}^3/\text{s}$, $Q_{bI} = 0.39 \text{ m}^3/\text{s}$, and $Q_{bH} = 0.82 \text{ m}^3/\text{s}$, corresponding to low, intermediate, and high base flow, respectively. The total runoff volume (R) is partitioned into the fraction of infiltration-excess runoff ($F_I = R_I/R$), saturation-excess runoff ($F_S = R_S/R$), perched return flow ($F_P = R_P/R$) and groundwater exfiltration ($F_G = R_G/R$). R^* is the total runoff for the particular case normalized by the total runoff from the Original surface.

Figure 5c shows the surface runoff difference $\Delta(r_I + r_S)$ between the Convex and Concave basins, indicating the impact of basin hypsometry. The Convex basin has higher surface runoff in small, rugged valleys (c1), while the Concave surface has higher ($r_I + r_S$) in floodplain regions along the main reach (c2). Spatially extensive differences in

($r_I + r_S$) are also present in upland areas with large elevation changes (c3). In effect, surface runoff generation sites shift in spatial location toward broad valleys for the more eroded Concave basin, while surface runoff in the Convex basin is focused in uplands. Figure 5d shows the differences in subsurface runoff $\Delta(r_P + r_G)$ in seepage lines where the

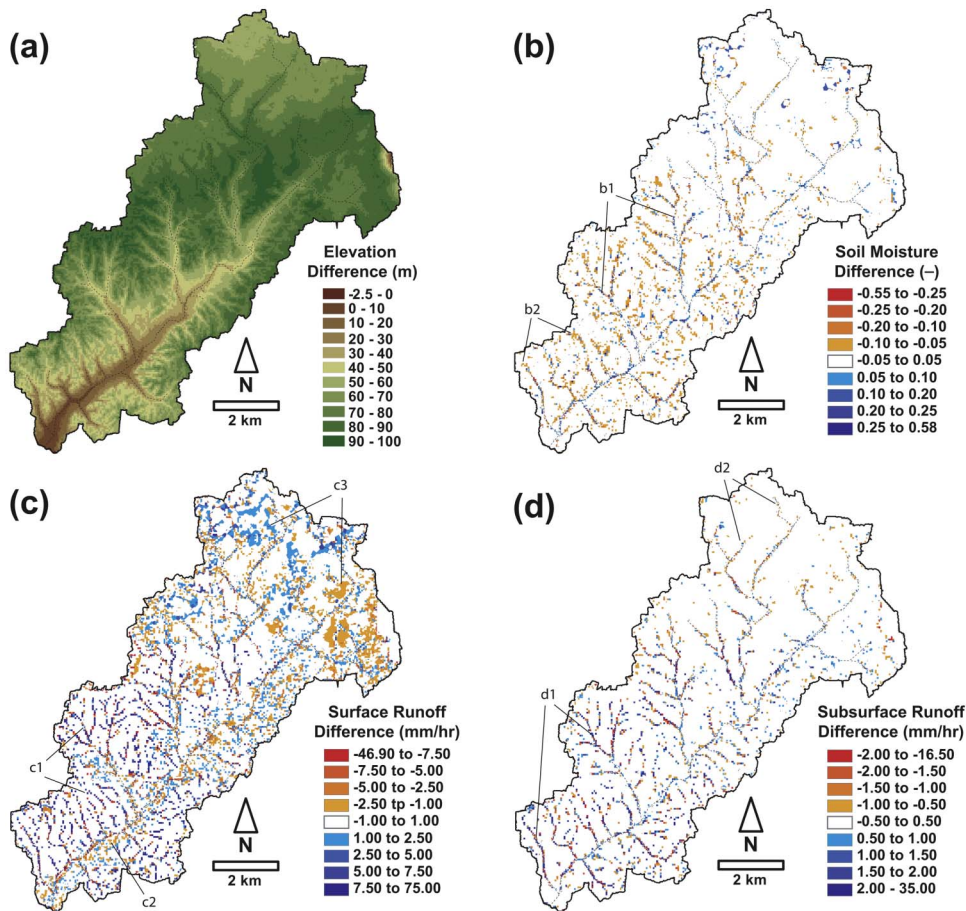


Figure 5. Spatial distribution of the differences in hydrological response in the Convex and Concave surfaces. For each variable (x), the difference (Δx) is calculated as $\Delta x = x_{\text{Convex}} - x_{\text{Concave}}$. Labels in each subplot indicate examples of the differences observed for each variable (see text for details). (a) Difference in surface elevation, Δz (m). (b) Difference in time-averaged surface soil moisture (top 10 cm), expressed as the degree of saturation (s is dimensionless and ranges from 0 to 1), Δs (–) over the 1-year simulation. (c) Difference in time-averaged surface runoff rate, $\Delta(r_I + r_S)$ (mm/hr). (d) Difference in time-averaged subsurface runoff rate, $\Delta(r_P + r_G)$ (mm/hr). For each component, the runoff rate (r in mm/hr) is averaged over the 1-year period. Negative Δx (red shades) imply higher x for the Concave surface, while positive Δx values (blue shades) are due to higher x for the Convex basin. For clarity, small differences (± 0.05 for Δs ; ± 1 mm/hr for $\Delta(r_I + r_S)$; and ± 0.5 mm/hr for $\Delta(r_P + r_G)$) are not shown.

water table intersects the land surface. Higher ($r_P + r_G$) for the Convex basin occurs in rugged valleys (d1), whereas the Concave basin has higher subsurface runoff in eroded uplands (d2). Seepage lines extending beyond the channel network represent the groundwater drainage density as noted by Marani et al. [2001] using a steady state groundwater model. This expansion suggests the channel extents may be tied to the hypsometric form (assumed constant here). Small tributaries in narrow valleys exhibit more pronounced $\Delta(r_P + r_G)$, suggesting that hypsometry has a strong local influence on water table and land surface interactions.

4. Discussion and Conclusions

[23] In this study, we utilize a distributed watershed model to identify the impact of the basin hypsometric form on surface and subsurface runoff processes in the Peacheater Creek basin, Oklahoma, for a 1-year study period. Relative to the Original surface, a less eroded Convex basin exhibits higher total runoff with larger contributions from subsurface processes, while a more eroded Concave basin has less total runoff with a higher fraction of surface response. The major shift in runoff production mechanisms is associated with higher infiltration and saturation-excess runoff ($R_I + R_S$) for the Concave basin along flatter regions near the basin outlet. This is primarily due to the shallower water table positions (leading to R_S) and lower surface gradients (leading to R_I). The relative location of the water table with respect to the land surface can amplify the hypsometric differences in runoff partitioning as the groundwater and variable source area rating curves are shown to be highly nonlinear. The basin hypsometric form also impacts the spatial distribution of soil moisture and runoff generation with a clear shift toward higher surface runoff along broad valleys for more eroded (Concave) basins.

[24] While the study is limited to three realizations of a single basin, the numerical experiments isolate the hypsometric effects by controlling other important factors (e.g., initial conditions, channel network density, bedrock depth, soil and vegetation cover). Clearly, these factors are interrelated in natural basins. For example, the dominant vegetation type or the channel network extent may change in response to long-term variations in the area-altitude relation. Nevertheless, the study results clearly reveal that the effect of the basin hypsometric form on the lumped and distributed basin response is through alterations in the underlying runoff mechanisms. Larger differences in basin hydrology would be expected for greater observed variations in the hypsometric distribution than those imposed in this study. In natural basins, we also expect differences in the hypsometric control on runoff response due to climate variability. In our study period, we confirmed that hypsometric trends at the annual scale were preserved for individual events. Longer term simulations would be desirable to further explore this issue.

[25] This work expands upon previous numerical modeling studies, while confirming trends presented by Luo [2000], Marani et al. [2001] and Bertoldi et al. [2006] in different climatic and physiographic regions. For example, Bertoldi et al. [2006] and our study both found that decreases in the hypsometric integral for Concave (eroded) basins yield lower total runoff with a higher surface contri-

but ion. Nevertheless, we show that the hypsometric distribution influences the basin water balance and runoff partitioning for a constant relief ratio. This differs from Bertoldi et al. [2006] who showed similar sensitivities of the hydrologic response for different basin relief ratios. Clearly, these numerical model investigations yield valuable insight into the variations in the basin response for different topographic settings that need to be further investigated through field studies. On the basis of this evidence, the hypsometric distribution and its statistical properties are considered useful metrics for inferring changes in basin runoff response, which may result from landscape evolution. Quantifying the relation between basin hypsometry and runoff partitioning may also lead to classifications of hydrologic response based on readily available topographic data and improved interpretation of long-term runoff records. Additional studies are required to characterize the impact of climate, soil and vegetation variations on the hypsometric control on surface and subsurface runoff.

[26] **Acknowledgments.** We acknowledge the comments of three anonymous reviewers that helped improve earlier versions of the manuscript. We also thank Valeriy Ivanov and Rafael L. Bras for contributions to the development of the tRIBS distributed hydrological model.

References

- Bertoldi, G., R. Rigon, and T. M. Over (2006), Impact of watershed geomorphic characteristics on the energy and water budgets, *J. Hydrometeorol.*, *7*, 389–403, doi:10.1175/JHM500.1.
- Duffy, C. J. (1996), A two-state integral-balance model for soil moisture and groundwater dynamics in complex terrain, *Water Resour. Res.*, *32*, 2421–2424, doi:10.1029/96WR01049.
- Eltahir, E. A. B., and P. J.-F. Yeh (1999), On the asymmetric response of aquifer water level to floods and droughts in Illinois, *Water Resour. Res.*, *35*, 1199–1217, doi:10.1029/1998WR900071.
- Harlin, J. M. (1978), Statistical moments of the hypsometric curve and its density function, *Math. Geol.*, *10*, 59–72, doi:10.1007/BF01033300.
- Harlin, J. M. (1984), Watershed morphometry and time to hydrograph peak, *J. Hydrol.*, *67*, 141–154, doi:10.1016/0022-1694(84)90238-5.
- Howard, A. D. (1990), Role of hypsometry and planform in basin hydrologic response, *Hydrol. Processes*, *4*, 373–385, doi:10.1002/hyp.3360040407.
- Hutchinson, M. (1989), A new procedure for gridding elevation and stream line data with automatic removal of spurious pits, *J. Hydrol.*, *106*, 211–232, doi:10.1016/0022-1694(89)90073-5.
- Ijjász-Vásquez, E. D., R. L. Bras, and G. E. Moglen (1992), Sensitivity of a basin evolution model to the nature of the runoff production and to initial conditions, *Water Resour. Res.*, *28*, 2733–2741, doi:10.1029/92WR01561.
- Imes, J. L., and L. F. Emmett (1994), Geohydrology of the Ozark Plateaus aquifer system in parts of Missouri, Arkansas, Oklahoma, and Kansas, *U.S. Geol. Surv. Prof. Pap.*, *1414-D*, 127 pp.
- Ivanov, V. Y., E. R. Vivoni, R. L. Bras, and D. Entekhabi (2004a), Catchment hydrologic response with a fully distributed triangulated irregular network model, *Water Resour. Res.*, *40*, W11102, doi:10.1029/2004WR003218.
- Ivanov, V. Y., E. R. Vivoni, R. L. Bras, and D. Entekhabi (2004b), Preserving high-resolution surface and rainfall data in operational-scale basin hydrology: A fully-distributed, physically-based approach, *J. Hydrol.*, *298*, 80–111, doi:10.1016/j.jhydrol.2004.03.041.
- Langbein, W. B., et al. (1947), Topographic characteristics of drainage basins, *U.S. Geol. Surv. Water Supply Pap.*, *968-C*, 125–155.
- Latron, J., and F. Gallart (2007), Seasonal dynamics of runoff-contributing areas in a small Mediterranean research catchment (Vallcebre, eastern Pyrenees), *J. Hydrol.*, *335*, 194–206, doi:10.1016/j.jhydrol.2006.11.012.
- Luo, W. (1998), Hypsometric analysis with a geographic information system, *Comput. Geosci.*, *24*, 815–821, doi:10.1016/S0098-3004(98)00076-4.
- Luo, W. (2000), Quantifying groundwater-sapping landforms with a hypsometric technique, *J. Geophys. Res.*, *105*, 1685–1694, doi:10.1029/1999JE001096.

- Luo, W., and J. M. Harlin (2003), A theoretical travel time based on watershed hypsometry, *J. Am. Water Resour. Assoc.*, *39*, 785–792, doi:10.1111/j.1752-1688.2003.tb04405.x.
- Marani, M., E. Eltahir, and A. Rinaldo (2001), Geomorphic controls on regional base flow, *Water Resour. Res.*, *37*, 2619–2630, doi:10.1029/2000WR000119.
- Moglen, G. E., and R. L. Bras (1995), The effect of spatial heterogeneities on geomorphic expression in a model of basin evolution, *Water Resour. Res.*, *31*, 2613–2623, doi:10.1029/95WR02036.
- Ohmori, H. (1993), Changes in the hypsometric curve through mountain building resulting from concurrent tectonics and denudation, *Geomorphology*, *8*, 263–277, doi:10.1016/0169-555X(93)90023-U.
- Reed, S., V. Koren, M. Smith, Z. Zhang, F. Moreda, D. J. Seo, and DMIP Participants (2004), Overall distributed model intercomparison project results, *J. Hydrol.*, *298*, 27–60, doi:10.1016/j.jhydrol.2004.03.031.
- Rodríguez-Iturbe, I., and J. B. Valdes (1979), The geomorphologic structure of the hydrologic response, *Water Resour. Res.*, *15*, 1409–1420, doi:10.1029/WR015i006p01409.
- Schumm, S. A. (1956), Evolution of drainage systems and slopes in badlands at Perth Amboy, New Jersey, *Geol. Soc. Am. Bull.*, *67*, 597–646, doi:10.1130/0016-7606(1956)67[597:EODSAS]2.0.CO;2.
- Strahler, A. N. (1952), Hypsometric (area-altitude) analysis of erosional topography, *Geol. Soc. Am. Bull.*, *63*, 1117–1142, doi:10.1130/0016-7606(1952)63[1117:HAAOET]2.0.CO;2.
- Tarboton, D. G., R. L. Bras, and I. Rodríguez-Iturbe (1992), A physical basis for drainage density, *Geomorphology*, *5*, 59–76, doi:10.1016/0169-555X(92)90058-V.
- Tucker, G. E., and R. L. Bras (1998), Hillslope processes, drainage density, and landscape morphology, *Water Resour. Res.*, *34*, 2751–2764, doi:10.1029/98WR01474.
- Vivoni, E. R., V. Y. Ivanov, R. L. Bras, and D. Entekhabi (2004), Generation of triangulated irregular networks based on hydrological similarity, *J. Hydrol. Eng.*, *9*, 288–302, doi:10.1061/(ASCE)1084-0699(2004)9:4(288).
- Vivoni, E. R., V. Y. Ivanov, R. L. Bras, and D. Entekhabi (2005), On the effects of triangulated terrain resolution on distributed hydrologic model response, *Hydrol. Processes*, *19*, 2101–2122, doi:10.1002/hyp.5671.
- Vivoni, E. R., D. Entekhabi, R. L. Bras, and V. Y. Ivanov (2007), Controls on runoff generation and scale-dependence in a distributed hydrologic model, *Hydrol. Earth Syst. Sci.*, *11*, 1683–1701.
- Willgoose, G. (1994), A statistic for testing the elevation characteristics of landscape simulation models, *J. Geophys. Res.*, *99*, 13,987–13,996, doi:10.1029/94JB00123.
- Willgoose, G., and G. Hancock (1998), Revisiting the hypsometric curve as an indicator of form and process in transport-limited catchment, *Earth Surf. Processes Landforms*, *23*, 611–623, doi:10.1002/(SICI)1096-9837(199807)23:7<611::AID-ESP872>3.0.CO;2-Y.
- Zecharias, Y. B., and W. Brutsaert (1988), The influence of basin morphology on groundwater outflow, *Water Resour. Res.*, *24*, 1645–1650, doi:10.1029/WR024i010p01645.

F. Di Benedetto and E. R. Vivoni, Department of Earth and Environmental Science, New Mexico Institute of Mining and Technology, 801 Leroy Place, MSEC 244, Socorro, NM 87801, USA. (vivoni@nmt.edu)

E. A. B. Eltahir, Department of Civil and Environmental Engineering, Massachusetts Institute of Technology, 77 Massachusetts Avenue, Cambridge, MA 02139, USA.

S. Grimaldi, Dipartimento di Geologia e Ingegneria Meccanica, Naturalistica e Idraulica per il Territorio, Università degli Studi della Tuscia, Via Camillo De Lellis, Viterbo I-01100, Italy.